ELSEVIER

Engineering Analysis with Boundary Elements 28 (2004) 1069–1082

ENGINEERING ANALYSIS *with* BOUNDARY ELEMENTS

www.elsevier.com/locate/enganabound

Three-dimensional Green's functions of steady-state motion in anisotropic half-spaces and bimaterials☆

B. Yang[a,*], E. Pan[b], V.K. Tewary[a]

[a]*Materials Reliability Division, National Institute of Standards and Technology, Boulder, CO 80305 USA*
[b]*Department of Civil Engineering, The University of Akron, Akron, OH 44325-3905, USA*

Received 22 July 2003; revised 20 January 2004; accepted 15 March 2004

Available online 2 June 2004

Abstract

Three-dimensional Green's functions (GFs) of steady-state motion in linear anisotropic elastic half-space and bimaterials are derived within the framework of generalized Stroh formalism and two-dimensional Fourier transforms. The present study is limited to the subsonic case where the sextic equation has six complex eigenvalues. If the source and field points reside in the same material, the GF is expressed in two parts: a singular part that corresponds to the infinite-space GF, and a complementary part that corresponds to the reflective effects of the interface in the bimaterial case and of the free surface in the half-space case. The singular part in the physical domain is calculated analytically by applying the Radon transform and the residue theorem. If the source and field points reside in different materials (in the bimaterial case), the GF is a one-term solution. The physical counterparts of the complementary part in the half-space case and of the one-term solution in the bimaterial case are derived as a one-dimensional integral by analytically carrying out the integration along the radial direction in the Fourier-inverse transform. When the source and field points are both on the interface in the bimaterial case or on the surface in the half-space case, singularities appear in the Fourier-inverse transform of the GF. The singularities are treated explicitly using a method proposed recently by the authors. Numerical examples are presented to demonstrate the effects of wave velocity on the stress fields, which may be of interest in various engineering problems of steady-state motion. Furthermore, these GFs are required in the steady-state boundary-integral-equation formulation of anisotropic elasticity.

Keywords: Anisotropy; Elastodynamics; Generalized Stroh formalism; Steady-state motion; Three-dimensional Green's function

1. Introduction

Green's function (GF) has been an interesting subject of research due to its direct and indirect applications to various engineering and physics problems. While most static GFs in anisotropic elastic and two-dimensional (2D) domains can be derived in terms of the Stroh formalism as given in Ref. [1], the three-dimensional (3D) static GFs were obtained by making use of the generalized Stroh formalism and 2D Fourier transforms [2–5]. Other techniques have also been applied to derive the static GFs in bimaterials and multilayered materials [6–8]. Development of the GFs under either general transient or time-harmonic (i.e. proportional to $e^{i\omega t}$) conditions poses great difficulty, as is evidenced in Refs. [9–11].

As is well known, a steady-state motion in velocity $\mathbf{v}$ is defined as the motion where the response depends on the combination of the space ($\mathbf{x}$) and time (t) variables as $\mathbf{x} - \mathbf{v}t$, instead of depending upon them individually. Such motions occur in many practical problems, such as moving cars on the highway and high-speed trains on the railway [12,13]. Recently, Verruijt and Cordova [14] presented a closed-form solution for the problem of a moving point load on an isotropic elastic half-plane with hysteretic damping. Lykotrafitis and Georgiadis [15] derived the 3D fundamental solution for a moving source on the surface of a thermo-elastic half-space. Andersen and Nielsen [16] presented a boundary-element analysis for the steady-state response of an elastic half-space subjected to a surface force. So far, however, very little has been done along these

☆ Publication of the National Institute of Standards and Technology, an agency of the US Government; not subject to copyright.

* Corresponding author. Address: Dept. of Mech. and Aerospace Engr., Florida Tech., Melbourne, FL 32901, USA. Tel.: +1-61-321-674-7713; fax: +1-61-321-674-8813.

E-mail address: boyang@fit.edu (B. Yang).

0955-7997/$ - see front matter © 2004 Elsevier Ltd. All rights reserved.
doi:10.1016/j.enganabound.2004.03.004

lines when the material is anisotropic [1]. The steady-state GFs for 3D anisotropic elastic media are not available in the literature.

In this paper, we apply the generalized Stroh formalism and 2D Fourier transforms to derive such steady-state GFs in anisotropic linearly elastic half-spaces and bimaterials. In the bimaterial case, the interface is perfectly bonded. In the half-space case, the surface is traction-free. The boundary-value problem of these systems subjected to a point force is first solved analytically in the Fourier-transformed domain. The physical-domain counterpart is then derived using the Fourier-inverse transform. The present study is limited to the subsonic case where the sextic equation has six complex eigenvalues. The formulation is described in Section 2. In Section 3, the GFs of half-space and bimaterials are derived. These GFs in the physical domain are expressed as a 1D integral over a finite interval. In Section 4, the special cases of both source and field points being located on the interface in the bimaterial case and on the surface in the half-space case are treated, where the 1D integral exhibits singularities. The singularities are treated explicitly using a method proposed recently by the authors [17]. In Section 5, numerical results of AlN/InN bimaterials are reported, demonstrating the validity and elegance of the present formulation, as well as the effects of wave velocity on the stress fields. Conclusions are drawn in Section 6.

2. Formulation

We consider a full space consisting of two semi-infinite homogenous materials, as shown in Fig. 1. The materials are linear anisotropic elastic, and the interface is perfectly bonded. A Cartesian coordinate system (x_1, x_2, x_3) is attached to the bimaterial structure, with the origin (0, 0, 0) located on the interface and the $(x_1 - x_2)$ plane coinciding with the interfacial plane. The material occupying $x_3 < 0$ is called material 1, and that occupying $x_3 > 0$ is called material 2. When one of the materials has zero stiffness, i.e. one of the half-spaces is empty, the bimaterial system is reduced to a half-space. We assume a point force $\mathbf{f}$ moving horizontally at a constant velocity $\mathbf{v}(= v_1, v_2, 0)$ in the space. The location of the point force is given by $\mathbf{X}_0 + \mathbf{v}t$, where t is the time and $\mathbf{X}_0$ is the initial location when $t = 0$.

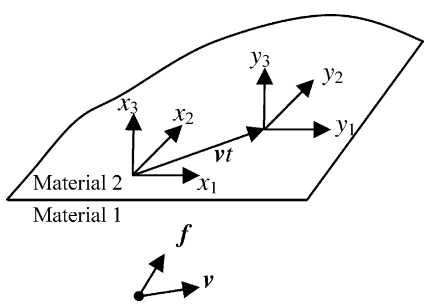

Fig. 1. A bimaterial infinite space subjected to a steadily moving point force $\mathbf{f}$ at velocity $\mathbf{v} = (v_1, v_2, 0)$.

The local constitutive law and the equation of motion of the structure are given by

$$\sigma_{ji} = C_{jilm} u_{l,m}, \tag{1}$$

$$\sigma_{ji,j} + f_i \delta(\mathbf{x} - \mathbf{X}_0 - \mathbf{v}t) = \rho \ddot{u}_i, \tag{2}$$

where σ_{ji} is the stress component, C_{jilm} is the elastic stiffness component, ρ is the mass density, $\delta(\mathbf{x})$ is the Dirac delta function, the dots over $\mathbf{u}$ indicate partial derivatives with respect to t, and the comma in the subscript indicates the partial derivative with respect to the coordinate that follows. The elastic stiffness and mass density are in general different in the two half-spaces. The Latin indices range from 1 to 3. Greek indices that will be used later range from 1 to 2. The repeated subscript implies the conventional summation over its range.

For a steady-state motion due to the point force $\mathbf{f}$ moving at a constant velocity $\mathbf{v}$, the displacement field $\mathbf{u}$ can be written as

$$u_i(\mathbf{x}, t) = u_i(\mathbf{x} - \mathbf{v}t). \tag{3}$$

Substituting Eqs. (1) and (3) into Eq. (2), the equations of motion become

$$C^*_{jilm} u_{l,mj} = -f_i \delta(\mathbf{y} - \mathbf{Y}), \tag{4}$$

where $C^*_{jilm} \equiv C_{jilm} - \rho v_m v_j \delta_{il}$, $\mathbf{Y} = \mathbf{X}_0$, and $\mathbf{y}(\equiv \mathbf{x} - \mathbf{v}t)$ is a new moving reference frame. The effective stiffness matrix C^*_{jilm} is not as fully symmetric as the stiffness matrix C_{jilm}. Otherwise, Eq. (4) resembles the equilibrium equation in elastostatics [1].

The continuity conditions of displacement and traction at the interface are given by

$$\mathbf{u}_1 = \mathbf{u}_2 \text{ and } \mathbf{t}_1 = \mathbf{t}_2 \text{ at } y_3 = 0, \tag{5}$$

where the subscripts 1 and 2 indicate the association of a quantity to materials 1 and 2, respectively, and $\mathbf{t}(\equiv (\sigma_{13}, \sigma_{23}, \sigma_{33})^{\mathrm{T}})$ consists of the stress components out of the interface plane, where the superscript T indicates the transpose of the matrix.

In addition, it is required physically that as $|\mathbf{y}|$ approaches infinity, the displacement $\mathbf{u}$ vanishes, i.e.

$$\lim_{|y| \to \infty} \mathbf{u}(\mathbf{y}) = 0. \tag{6}$$

This is called the radiation condition. This condition may not be satisfied by all solutions of steady-state motion at arbitrary velocity $\mathbf{v}$ that are mathematically permissible to Eqs. (4) and (5). The present study is limited to the case where Eq. (6) holds.

3. Bimaterial and half-space Green's functions

3.1. General solution in Stroh formalism

Within the generalized Stroh formalism, we first apply the following 2D Fourier transforms (k_1, k_2) to the in-plane variables of $u_i(y)$ as

$$\tilde{u}_i(k_1, k_2, y_3) = \int\int u_i(y_1, y_2, y_3) \mathrm{e}^{ik_\alpha y_\alpha} \mathrm{d}y_1 \mathrm{d}y_2, \tag{7}$$

where e stands for the *exponential* function, and i in the exponent denotes the unit of imaginary number, $\sqrt{-1}$. The integral limits are $(-\infty, \infty)$ in both coordinates y_1 and y_2. Thus, in the Fourier-transformed domain, the equation of motion, Eq. (4), becomes

$$C^*_{3ik3}\tilde{u}_{k,33} - i(C^*_{\alpha ik3} + C^*_{3ik\alpha})k_\alpha \tilde{u}_{k,3} - C^*_{\alpha ik\beta}k_\alpha k_\beta \tilde{u}_k = -f_i \mathrm{e}^{iY_\alpha k_\alpha}\delta(Y_3). \tag{8}$$

Solving the above ordinary differential equation yields a general solution as

$$\tilde{\mathbf{u}}(k_1, k_2, y_3) = \mathbf{a}\mathrm{e}^{-ip\eta y_3}, \tag{9}$$

where η is the norm of $(k_1 = \eta\cos\theta, k_2 = \eta\sin\theta)$, and p and $\mathbf{a}$ satisfy the eigenrelation

$$[\mathbf{Q} + p(\mathbf{R} + \mathbf{R}^{\mathrm{T}}) + p^2\mathbf{T}]\mathbf{a} = 0, \tag{10}$$

with

$$Q_{ik} = C^*_{\alpha ik\beta}n_\alpha n_\beta, \qquad R_{ik} = C^*_{\alpha ik3}n_\alpha, \qquad T_{IK} = C^*_{3ik3}. \tag{11}$$

In the above equation, $n_1 = \cos\theta$, and $n_2 = \sin\theta$, where θ together with η are the polar coordinates of the transformed plane (k_1, k_2).

Besides vector $\mathbf{t}$, we define another vector consisting of the stress components in the horizontal plane as $s \equiv (\sigma_{11}, \sigma_{12}, \sigma_{22})^{\mathrm{T}}$. The combination of $\mathbf{t}$ and $\mathbf{s}$ represents the complete stress tensor σ because of its symmetry. Utilizing the constitutive law in Eq. (1) and applying the 2D Fourier transform in Eq. (7), these vectors are obtained in the transformed domain as

$$\tilde{\mathbf{t}} = -i\eta\mathbf{b}\,\mathrm{e}^{-ip\eta y_3}, \tag{12}$$

$$\tilde{\mathbf{s}} = -i\eta\mathbf{c}\,\mathrm{e}^{-ip\eta y_3}, \tag{13}$$

where

$$b_i = (C_{3ik\alpha}n_\alpha + pC_{3ik3})a_k, \tag{14}$$

$$c_1 = (C_{11k\alpha}n_\alpha + pC_{11k3})a_k,$$

$$c_2 = (C_{12k\alpha}n_\alpha + pC_{12k3})a_k, \tag{15}$$

$$c_3 = (C_{22k\alpha}n_\alpha + pC_{22k3})a_k.$$

Depending upon the values of the stiffness constants C_{jilm} and point-force velocity $\mathbf{v}$, the eigenvalues p of Eq. (10) may be complex or real. In the following, we confine our discussion to the case where all the eigenvalues of Eq. (10) are complex. In this case, the eigenvalues p_i and associated eigenvectors a_i, b_i and c_i appear in pairs of complex conjugates. We arrange these eigenvalues and eigenvectors in the following way:

$$\mathrm{Im}\, p_i > 0,\ p_{i+3} = \bar{p}_i,\ \mathbf{a}_{i+3} = \bar{\mathbf{a}}_i,\ \mathbf{b}_{i+3} = \bar{\mathbf{b}}_i,$$
$$\mathbf{c}_{i+3} = \bar{\mathbf{c}}_i\ \ (i = 1, 2, 3) \tag{16}$$

$$\mathbf{A} = [\mathbf{a}_1, \mathbf{a}_2, \mathbf{a}_3],\ \ \mathbf{B} = [\mathbf{b}_1, \mathbf{b}_2, \mathbf{b}_3],\ \ \mathbf{C} = [\mathbf{c}_1, \mathbf{c}_2, \mathbf{c}_3], \tag{17}$$

where *Im* stands for the imaginary part and the overbar denotes the complex conjugate. Assuming that $p_i (i = 1, 2, 3)$ are distinct, the general solutions of displacement and stress are obtained by superposing the six solutions of Eqs. (9), (12) and (13), respectively, as

$$\tilde{\mathbf{u}} = i\eta^{-1}\bar{\mathbf{A}}\langle \mathrm{e}^{-i\bar{p}\eta y_3}\rangle \mathbf{q} + i\eta^{-1}\mathbf{A}\langle \mathrm{e}^{-ip\eta y_3}\rangle \mathbf{w}, \tag{18}$$

$$\tilde{\mathbf{t}} = \bar{\mathbf{B}}\langle \mathrm{e}^{-i\bar{p}\eta y_3}\rangle \mathbf{q} + \mathbf{B}\langle \mathrm{e}^{-ip\eta y_3}\rangle \mathbf{w}, \tag{19}$$

$$\tilde{\mathbf{s}} = \bar{\mathbf{C}}\langle \mathrm{e}^{-i\bar{p}\eta y_3}\rangle \mathbf{q} + \mathbf{C}\langle \mathrm{e}^{-ip\eta y_3}\rangle \mathbf{w}, \tag{20}$$

where $\mathbf{q}(k_1, k_2)$ and $\mathbf{w}(k_1, k_2)$ are unknown complex vectors and

$$\langle \mathrm{e}^{-ip\eta y_3}\rangle = \mathrm{diag}[\mathrm{e}^{-ip_1\eta y_3},\ \mathrm{e}^{-ip_2\eta y_3},\ \mathrm{e}^{-ip_3\eta y_3}]. \tag{21}$$

Note that the above matrix $\mathbf{C}$ is different from the fourth-order elastic stiffness tensor C_{ijkl}.

The above derivation is applicable to a homogeneous domain. When applying the solutions in Eqs. (18)–(20) to the bimaterial system (Fig. 1), two sets of unknown vectors $(\mathbf{q}_1, \mathbf{w}_1)$ and $(\mathbf{q}_2, \mathbf{w}_2)$ result. These unknowns can be determined by imposing the interfacial and radiation conditions of Eqs. (5) and (6), and the continuity condition of displacement and jump condition of stress at the location where the moving point force $\mathbf{f}$ is applied. Once the solution for the transformed domain is derived, the physical-domain GF due to a point force $\mathbf{f}$ is obtained by applying the Fourier-inverse transform, for instance, of u_i, as

$$u_i(y_1, y_2, y_3) = \frac{1}{(2\pi)^2}\int\int \tilde{u}_i(k_1, k_2, y_3)\mathrm{e}^{-ik_\alpha y_\alpha}\mathrm{d}k_1\mathrm{d}k_2, \tag{22}$$

where the integral limits in both coordinates are from $-\infty$ to ∞. Alternatively, the inverse transform can be carried out in polar coordinates,

$$u_i(y_1, y_2, y_3) = \frac{1}{(2\pi)^2}\int\int \eta\tilde{u}_i(k_1, k_2, y_3)\mathrm{e}^{-ik_\alpha y_\alpha}\mathrm{d}\eta\mathrm{d}\theta, \tag{23}$$

where the integral limit of η is from 0 to ∞, and that of θ is from 0 to 2π.

3.2. Bimaterial Green's function

Now we write the transformed-domain GFs for bimaterials as

$$\tilde{\mathbf{u}}_m(k_1, k_2, y_3)\mathrm{e}^{-ik_\alpha Y_\alpha} = \tilde{\mathbf{u}}^{(s)}_m(k_1, k_2, y_3) + i\eta^{-1}\bar{\mathbf{A}}_m\langle \mathrm{e}^{-i\bar{p}_m\eta y_3}\rangle \mathbf{q}_m + i\eta^{-1}\mathbf{A}_m\langle \mathrm{e}^{-ip_m\eta y_3}\rangle \mathbf{w}_m, \tag{24}$$

$$\tilde{\mathbf{t}}_m(k_1,k_2,y_3)\mathrm{e}^{-ik_\alpha Y_\alpha} = \tilde{\mathbf{t}}_m^{(s)}(k_1,k_2,y_3) + \bar{\mathbf{B}}_m\langle \mathrm{e}^{-i\bar{p}_m\eta y_3}\rangle \mathbf{q}_m + \mathbf{B}_m\langle \mathrm{e}^{-ip_m\eta y_3}\rangle \mathbf{w}_m, \tag{25}$$

$$\tilde{\mathbf{s}}_m(k_1,k_2,y_3)\mathrm{e}^{-ik_\alpha Y_\alpha} = \tilde{\mathbf{s}}_m^{(s)}(k_1,k_2,y_3) + \bar{\mathbf{C}}_m\langle \mathrm{e}^{-i\bar{p}_m\eta y_3}\rangle \mathbf{q}_m + \mathbf{C}_m\langle \mathrm{e}^{-ip_m\eta y_3}\rangle \mathbf{w}_m, \tag{26}$$

where the subscript m (= 1, 2) indicates the association of a quantity to material 1 or 2, and $\tilde{\mathbf{u}}_m^{(s)}$, $\tilde{\mathbf{t}}_m^{(s)}$ and $\tilde{\mathbf{s}}_m^{(s)}$ are special solutions to be given. Once the unknown vectors $(\mathbf{q}_m, \mathbf{w}_m)$ are determined, the bimaterial GFs are obtained.

To solve the problem, we take the special solutions to be the infinite-space GFs of the material where the point force $\mathbf{f}$ is located, and to be equal to zero in the other material. The infinite-space GFs are given by

$$\tilde{\mathbf{u}}^{(\infty)}(k_1,k_2,y_3) = \begin{cases} i\eta^{-1}\mathbf{A}\langle \mathrm{e}^{-ip\eta(y_3-Y_3)}\rangle \mathbf{q}^{(\infty)}, & y_3 < Y_3 \\ -i\eta^{-1}\bar{\mathbf{A}}\langle \mathrm{e}^{-i\bar{p}\eta(y_3-Y_3)}\rangle \bar{\mathbf{q}}^{(\infty)}, & y_3 > Y_3 \end{cases}, \tag{27}$$

$$\tilde{\mathbf{t}}^{(\infty)}(k_1,k_2,y_3) = \begin{cases} \mathbf{B}\langle \mathrm{e}^{-ip\eta(y_3-Y_3)}\rangle \mathbf{q}^{(\infty)}, & y_3 < Y_3 \\ -\bar{\mathbf{B}}\langle \mathrm{e}^{-i\bar{p}\eta(y_3-Y_3)}\rangle \bar{\mathbf{q}}^{(\infty)}, & y_3 > Y_3 \end{cases}, \tag{28}$$

$$\tilde{\mathbf{s}}^{(\infty)}(k_1,k_2,y_3) = \begin{cases} \mathbf{C}\langle \mathrm{e}^{-ip\eta(y_3-Y_3)}\rangle \mathbf{q}^{(\infty)}, & y_3 < Y_3 \\ -\bar{\mathbf{C}}\langle \mathrm{e}^{-i\bar{p}\eta(y_3-Y_3)}\rangle \bar{\mathbf{q}}^{(\infty)}, & y_3 > Y_3 \end{cases}. \tag{29}$$

where $\mathbf{q}^{(\infty)} = \mathbf{A}^{-1}(\mathbf{M}-\bar{\mathbf{M}})^{-1}\mathbf{f}$ with $\mathbf{M} = -i\mathbf{B}\mathbf{A}^{-1}$. Given the explicit special solution, the unknown vectors $(\mathbf{q}_m, \mathbf{w}_m)$ can be determined by imposing the conditions in Eqs. (5) and (6). Since the infinite-space GFs satisfy the condition of traction jump at the point-force location, the part of the solution in terms of $(\mathbf{q}_m, \mathbf{w}_m)$ is continuous across the point-force loading location. The infinite-space GFs also satisfy the radiation condition in Eq. (6).

In the case that $\mathbf{f}$ is located in material $1(Y_3 \le 0)$, the bimaterial GFs in the transformed domain are obtained as, for $y_3 \le 0$,

$$\tilde{\mathbf{u}}_1(k_1,k_2,y_3)\mathrm{e}^{-ik_\alpha Y_\alpha} = \tilde{\mathbf{u}}_1^{(\infty)}(k_1,k_2,y_3) - i\eta^{-1}\mathbf{A}_1\langle \mathrm{e}^{-ip_1\eta y_3}\rangle \mathbf{F}_{11}\langle \mathrm{e}^{i\bar{p}_1\eta Y_3}\rangle \bar{\mathbf{q}}_1^{(\infty)}, \tag{30}$$

$$\tilde{\mathbf{t}}_1(k_1,k_2,y_3)\mathrm{e}^{-ik_\alpha Y_\alpha} = \tilde{\mathbf{t}}_1^{(\infty)}(k_1,k_2,y_3) - \mathbf{B}_1\langle \mathrm{e}^{-ip_1\eta y_3}\rangle \mathbf{F}_{11}\langle \mathrm{e}^{i\bar{p}_1\eta Y_3}\rangle \bar{\mathbf{q}}_1^{(\infty)}, \tag{31}$$

$$\tilde{\mathbf{s}}_1(k_1,k_2,y_3)\mathrm{e}^{-ik_\alpha Y_\alpha} = \tilde{\mathbf{s}}_1^{(\infty)}(k_1,k_2,y_3) - \mathbf{C}_1\langle \mathrm{e}^{-ip_1\eta y_3}\rangle \mathbf{F}_{11}\langle \mathrm{e}^{i\bar{p}_1\eta Y_3}\rangle \bar{\mathbf{q}}_1^{(\infty)}, \tag{32}$$

where $\mathbf{F}_{11} = \mathbf{A}_1^{-1}(\bar{\mathbf{M}}_2 - \mathbf{M}_1)^{-1}(\bar{\mathbf{M}}_1 - \bar{\mathbf{M}}_2)\bar{\mathbf{A}}_1$, and for $y_3 \ge 0$,

$$\tilde{\mathbf{u}}_2(k_1,k_2,y_3)\mathrm{e}^{-ik_\alpha Y_\alpha} = -i\eta^{-1}\bar{\mathbf{A}}_2\langle \mathrm{e}^{-i\bar{p}_2\eta y_3}\rangle \mathbf{F}_{12}\langle \mathrm{e}^{i\bar{p}_1\eta Y_3}\rangle \bar{\mathbf{q}}_1^{(\infty)}, \tag{33}$$

$$\tilde{\mathbf{t}}_2(k_1,k_2,y_3)\mathrm{e}^{-ik_\alpha Y_\alpha} = -\bar{\mathbf{B}}_2\langle \mathrm{e}^{-i\bar{p}_2\eta y_3}\rangle \mathbf{F}_{12}\langle \mathrm{e}^{i\bar{p}_1\eta Y_3}\rangle \bar{\mathbf{q}}_1^{(\infty)}, \tag{34}$$

$$\tilde{\mathbf{s}}_2(k_1,k_2,y_3)\mathrm{e}^{-ik_\alpha Y_\alpha} = -\bar{\mathbf{C}}_2\langle \mathrm{e}^{-i\bar{p}_2\eta y_3}\rangle \mathbf{F}_{12}\langle \mathrm{e}^{i\bar{p}_1\eta Y_3}\rangle \bar{\mathbf{q}}_1^{(\infty)}, \tag{35}$$

where

$$\mathbf{F}_{12} = \bar{\mathbf{A}}_2^{-1}(\bar{\mathbf{M}}_2 - \mathbf{M}_1)^{-1}(\bar{\mathbf{M}}_1 - \mathbf{M}_1)\bar{\mathbf{A}}_1.$$

In the case that $\mathbf{f}$ is located in material $2(Y_3 \ge 0)$, the bimaterial GFs in the transformed domain are obtained, for $y_3 \le 0$, as

$$\tilde{\mathbf{u}}_1(k_1,k_2,y_3)\mathrm{e}^{-ik_\alpha Y_\alpha} = i\eta^{-1}\mathbf{A}_1\langle \mathrm{e}^{-ip_1\eta y_3}\rangle \mathbf{F}_{21}\langle \mathrm{e}^{ip_2\eta Y_3}\rangle \mathbf{q}_2^{(\infty)}, \tag{36}$$

$$\tilde{\boldsymbol{t}}_1(k_1,k_2,y_3)\mathrm{e}^{-ik_\alpha Y_\alpha} = \mathbf{B}_1\left\langle \mathrm{e}^{-i\mathbf{p}_1\eta y_3}\right\rangle \mathbf{F}_{21}\left\langle \mathrm{e}^{i\mathbf{p}_2\eta Y_3}\right\rangle \mathbf{q}_2^{(\infty)}, \tag{37}$$

$$\tilde{\mathbf{s}}_1(k_1,k_2,y_3)\mathrm{e}^{-ik_\alpha Y_\alpha} = \mathbf{C}_1\langle \mathrm{e}^{-ip_1\eta y_3}\rangle \mathbf{F}_{21}\langle \mathrm{e}^{ip_2\eta Y_3}\rangle \mathbf{q}_2^{(\infty)}, \tag{38}$$

where $\mathbf{F}_{21} = \mathbf{A}_1^{-1}(\mathbf{M}_1 - \bar{\mathbf{M}}_2)^{-1}(\mathbf{M}_2 - \bar{\mathbf{M}}_2)\mathbf{A}_2$, and for $y_3 \ge 0$,

$$\tilde{\mathbf{u}}_2(k_1,k_2,y_3)\mathrm{e}^{-ik_\alpha Y_\alpha} = \tilde{\mathbf{u}}_2^{(\infty)}(k_1,k_2,y_3) + i\eta^{-1}\bar{\mathbf{A}}_2\langle \mathrm{e}^{-i\bar{p}_2\eta y_3}\rangle \mathbf{F}_{22}\langle \mathrm{e}^{ip_2\eta Y_3}\rangle \mathbf{q}_2^{(\infty)}, \tag{39}$$

$$\tilde{\mathbf{t}}_2(k_1,k_2,y_3)\mathrm{e}^{-ik_\alpha Y_\alpha} = \tilde{\mathbf{t}}_2^{(\infty)}(k_1,k_2,y_3) + \bar{\mathbf{B}}_2\langle \mathrm{e}^{-i\bar{p}_2\eta y_3}\rangle \mathbf{F}_{22}\langle \mathrm{e}^{ip_2\eta Y_3}\rangle \mathbf{q}_2^{(\infty)}, \tag{40}$$

$$\tilde{\mathbf{s}}_2(k_1,k_2,y_3)\mathrm{e}^{-ik_\alpha Y_\alpha} = \tilde{\mathbf{s}}_2^{(\infty)}(k_1,k_2,y_3) + \bar{\mathbf{C}}_2\langle \mathrm{e}^{-i\bar{p}_2\eta y_3}\rangle \mathbf{F}_{22}\langle \mathrm{e}^{ip_2\eta Y_3}\rangle \mathbf{q}_2^{(\infty)}, \tag{41}$$

where $\mathbf{F}_{22} = \bar{\mathbf{A}}_2^{-1}(\mathbf{M}_1 - \bar{\mathbf{M}}_2)^{-1}(\mathbf{M}_2 - \mathbf{M}_1)\mathbf{A}_2$.

To obtain the physical-domain GFs, we apply the Fourier-inverse transform (23) to Eqs. (30)–(41). In the present case, these 2D integrals are reducible to a 1D integral over a finite interval by analytically carrying out the integration over the radial direction η [2]. The final expressions of the physical-domain GFs are given by

$$u_{1i}(\mathbf{y}) = u_{1i}^{(\infty)}(\mathbf{y}) - \frac{1}{4\pi^2}\int_0^{2\pi} \frac{A_{1ik}F_{11kl}\bar{q}_{1l}^{(\infty)}}{p_{1k}y_3 - \bar{p}_{1l}Y_3 + r\cos(\theta-\theta_0)}d\theta, \tag{42}$$

$$t_{1i}(\mathbf{y}) = t_{1i}^{(\infty)}(\mathbf{y}) + \frac{1}{4\pi^2}\int_0^{2\pi} \frac{B_{1ik}F_{11kl}\bar{q}_{1l}^{(\infty)}}{[p_{1k}y_3 - \bar{p}_{1l}Y_3 + r\cos(\theta-\theta_0)]^2}d\theta, \tag{43}$$

$$s_{1i}(\mathbf{y}) = s_{1i}^{(\infty)}(\mathbf{y}) + \frac{1}{4\pi^2}\int_0^{2\pi} \frac{C_{1ik}F_{11kl}\bar{q}_{1l}^{(\infty)}}{[p_{1k}y_3 - \bar{p}_{1l}Y_3 + r\cos(\theta-\theta_0)]^2}\mathrm{d}\theta, \tag{44}$$

$$u_{2i}(\mathbf{y}) = -\frac{1}{4\pi^2}\int_0^{2\pi} \frac{\bar{A}_{2ik}F_{12kl}\bar{q}_{1l}^{(\infty)}}{\bar{p}_{2k}y_3 - \bar{p}_{1l}Y_3 + r\cos(\theta-\theta_0)}\mathrm{d}\theta, \tag{45}$$

$$t_{2i}(\mathbf{y}) = \frac{1}{4\pi^2}\int_0^{2\pi} \frac{\bar{B}_{2ik}F_{12kl}\bar{q}_{1l}^{(\infty)}}{[\bar{p}_{2k}y_3 - \bar{p}_{1l}Y_3 + r\cos(\theta-\theta_0)]^2}\mathrm{d}\theta, \tag{46}$$

$$s_{2i}(\mathbf{y}) = \frac{1}{4\pi^2}\int_0^{2\pi} \frac{\bar{C}_{2ik}F_{12kl}\bar{q}_{1l}^{(\infty)}}{[\bar{p}_{2k}y_3 - \bar{p}_{1l}Y_3 + r\cos(\theta-\theta_0)]^2}\mathrm{d}\theta, \tag{47}$$

in the case that **f** is located in material 1 ($Y_3 \le 0$), and

$$u_{1i}(\mathbf{y}) = \frac{1}{4\pi^2}\int_0^{2\pi} \frac{A_{1ik}F_{21kl}q_{2l}^{(\infty)}}{p_{1k}y_3 - p_{2l}Y_3 + r\cos(\theta-\theta_0)}\mathrm{d}\theta, \tag{48}$$

$$t_{1i}(\mathbf{y}) = \frac{1}{4\pi^2}\int_0^{2\pi} \frac{-B_{1ik}F_{21kl}q_{2l}^{(\infty)}}{[p_{1k}y_3 - p_{2l}Y_3 + r\cos(\theta-\theta_0)]^2}\mathrm{d}\theta, \tag{49}$$

$$s_{1i}(\mathbf{y}) = \frac{1}{4\pi^2}\int_0^{2\pi} \frac{-C_{1ik}F_{21kl}q_{2l}^{(\infty)}}{[p_{1k}y_3 - p_{2l}Y_3 + r\cos(\theta-\theta_0)]^2}\mathrm{d}\theta, \tag{50}$$

$$u_{2i}(\mathbf{y}) = u_{2i}^{(\infty)}(\mathbf{y}) + \frac{1}{4\pi^2}\int_0^{2\pi} \frac{\bar{A}_{2ik}F_{22kl}q_{2l}^{(\infty)}}{\bar{p}_{2k}y_3 - p_{2l}Y_3 + r\cos(\theta-\theta_0)}\mathrm{d}\theta, \tag{51}$$

$$t_{2i}(\mathbf{y}) = t_{2i}^{(\infty)}(\mathbf{y}) + \frac{1}{4\pi^2}\int_0^{2\pi} \frac{-\bar{B}_{2ik}F_{22kl}q_{2l}^{(\infty)}}{[\bar{p}_{2k}y_3 - p_{2l}Y_3 + r\cos(\theta-\theta_0)]^2}\mathrm{d}\theta, \tag{52}$$

$$s_{2i}(\mathbf{y}) = s_{2i}^{(\infty)}(\mathbf{y}) + \frac{1}{4\pi^2}\int_0^{2\pi} \frac{-\bar{C}_{2ik}F_{22kl}q_{2l}^{(\infty)}}{[\bar{p}_{2k}y_3 - p_{2l}Y_3 + r\cos(\theta-\theta_0)]^2}\mathrm{d}\theta, \tag{53}$$

in the case that **f** is located in material 2($Y_3 \ge 0$). In the above expressions,

$$r = \sqrt{(y_1 - Y_1)^2 + (y_2 - Y_2)^2} \text{ and } \theta_0 = \sin^{-1}((y_2 - Y_2)/r). \tag{54}$$

The infinite-space GFs in the physical domain are obtained analytically by applying the Radon transform and the residue theorem, similar to the derivation for the static infinite-space GFs in anisotropic elastic and piezoelectric solids [18,19]. This is summarized in Appendix A.

3.3. Half-space Green's function

When one of the materials 1 and 2 has zero stiffness (i.e. when one of the half-spaces is empty), the bimaterial system is reduced to a half-space. In this case, eight different boundary conditions with combinations of either displacement or traction given in each component may be applied on the half-space surface. The different boundary conditions, together with the radiation condition of Eq. (6), would result in different half-space GFs. Only the one under the traction-free surface condition is given below. One may refer to [1,3,20] for a detailed treatment of the half-plane and half-space GFs under general boundary conditions in elastostatics and static piezoelectricity.

In the case of the lower half-space ($y_3 \le 0$), the transformed-domain GF under the traction-free surface condition ($\mathbf{t} = 0$ at $y_3 = 0$) is given by

$$\tilde{\mathbf{u}}(k_1,k_2,y_3)\mathrm{e}^{-ik_\alpha Y_\alpha} = \tilde{\mathbf{u}}^{(\infty)}(k_1,k_2,y_3) + i\eta^{-1}\mathbf{A}\langle \mathrm{e}^{-ip\eta y_3}\rangle \mathbf{B}^{-1}\bar{\mathbf{B}}\langle \mathrm{e}^{i\bar{p}\eta Y_3}\rangle \bar{\mathbf{q}}^{(\infty)}, \tag{55}$$

$$\tilde{\mathbf{t}}(k_1,k_2,y_3)\mathrm{e}^{-ik_\alpha Y_\alpha} = \tilde{\mathbf{t}}^{(\infty)}(k_1,k_2,y_3) + \mathbf{B}\langle \mathrm{e}^{-ip\eta y_3}\rangle \mathbf{B}^{-1}\bar{\mathbf{B}}\langle \mathrm{e}^{i\bar{p}\eta Y_3}\rangle \bar{\mathbf{q}}^{(\infty)}, \tag{56}$$

$$\tilde{\mathbf{s}}(k_1,k_2,y_3)\mathrm{e}^{-ik_\alpha Y_\alpha} = \tilde{\mathbf{s}}^{(\infty)}(k_1,k_2,y_3) + \mathbf{C}\langle \mathrm{e}^{-ip\eta y_3}\rangle \mathbf{B}^{-1}\bar{\mathbf{B}}\langle \mathrm{e}^{i\bar{p}\eta Y_3}\rangle \bar{\mathbf{q}}^{(\infty)}. \tag{57}$$

Following the same procedure as that previously used in the bimaterial system, the physical-domain half-space GF is derived as

$$u_i(\mathbf{y}) = u_i^{(\infty)}(\mathbf{y}) + \frac{1}{4\pi^2}\int_0^{2\pi} \frac{A_{ik}(\mathbf{B}^{-1}\bar{\mathbf{B}})_{kl}\bar{q}_l^{(\infty)}}{p_k y_3 - \bar{p}_l Y_3 + r\cos(\theta-\theta_0)}\mathrm{d}\theta, \tag{58}$$

$$t_i(\mathbf{y}) = t_i^{(\infty)}(\mathbf{y}) + \frac{1}{4\pi^2}\int_0^{2\pi} \frac{-B_{ik}(\mathbf{B}^{-1}\bar{\mathbf{B}})_{kl}\bar{q}_l^{(\infty)}}{[p_k y_3 - \bar{p}_l Y_3 + r\cos(\theta-\theta_0)]^2}\mathrm{d}\theta, \tag{59}$$

$$s_i(\mathbf{y}) = s_i^{(\infty)}(\mathbf{y}) + \frac{1}{4\pi^2}\int_0^{2\pi} \frac{-C_{ik}(\mathbf{B}^{-1}\bar{\mathbf{B}})_{kl}\bar{q}_l^{(\infty)}}{[p_k y_3 - \bar{p}_l Y_3 + r\cos(\theta-\theta_0)]^2}\mathrm{d}\theta. \tag{60}$$

In the case of the upper half-space ($y_3 \ge 0$), the transformed-domain GF under the traction-free surface condition is given by

$$\tilde{\mathbf{u}}(k_1,k_2,y_3)\mathrm{e}^{-ik_\alpha Y_\alpha} = \tilde{\mathbf{u}}^{(\infty)}(k_1,k_2,y_3) - i\eta^{-1}\bar{\mathbf{A}}\langle \mathrm{e}^{-i\bar{p}\eta y_3}\rangle \bar{\mathbf{B}}^{-1}\mathbf{B}\langle \mathrm{e}^{ip\eta Y_3}\rangle \mathrm{q}^{(\infty)}, \tag{61}$$

$$\tilde{\mathbf{t}}(k_1,k_2,y_3)\mathrm{e}^{-ik_\alpha Y_\alpha} = \tilde{\mathbf{t}}^{(\infty)}(k_1,k_2,y_3) - \bar{\mathbf{B}}\langle \mathrm{e}^{-i\bar{p}\eta y_3}\rangle \bar{\mathbf{B}}^{-1}\mathbf{B}\langle \mathrm{e}^{ip\eta Y_3}\rangle \mathbf{q}^{(\infty)}, \tag{62}$$

$$\tilde{\mathbf{s}}(k_1,k_2,y_3)\mathrm{e}^{-ik_\alpha Y_\alpha} = \tilde{\mathbf{s}}^{(\infty)}(k_1,k_2,y_3) - \bar{\mathbf{C}}\langle \mathrm{e}^{-i\bar{p}\eta y_3}\rangle \bar{\mathbf{B}}^{-1}\mathbf{B}\langle \mathrm{e}^{ip\eta Y_3}\rangle \mathbf{q}^{(\infty)}. \tag{63}$$

The corresponding physical-domain GF is given by

$$u_i(\mathbf{y}) = u_i^{(\infty)}(\mathbf{y}) - \frac{1}{4\pi^2}\int_0^{2\pi} \frac{\bar{A}_{ik}(\bar{\mathbf{B}}^{-1}\mathbf{B})_{kl}q_l^{(\infty)}}{\bar{p}_k y_3 - p_l Y_3 + r\cos(\theta-\theta_0)}\mathrm{d}\theta, \tag{64}$$

$$t_i(\mathbf{y}) = t_i^{(\infty)}(\mathbf{y}) + \frac{1}{4\pi^2}\int_0^{2\pi} \frac{\bar{B}_{ik}(\bar{\mathbf{B}}^{-1}\mathbf{B})_{kl}q_l^{(\infty)}}{[\bar{p}_k y_3 - p_l Y_3 + r\cos(\theta-\theta_0)]^2}\mathrm{d}\theta, \tag{65}$$

$$s_i(\mathbf{y}) = s_i^{(\infty)}(\mathbf{y}) + \frac{1}{4\pi^2}\int_0^{2\pi} \frac{\bar{C}_{ik}(\bar{\mathbf{B}}^{-1}\mathbf{B})_{kl}q_l^{(\infty)}}{[\bar{p}_k y_3 - p_l Y_3 + r\cos(\theta-\theta_0)]^2}\mathrm{d}\theta. \tag{66}$$

4. Interfacial and surface Green's functions

4.1. Interfacial Green's function

When the source point (i.e. the point force **f**) is located on the interface, the GF is called the interfacial GF [1]. If only the source point is located on the interface (but the field point is not!), the expressions of the physical-domain steady-state bimaterial GFs derived above are nonsingular. Thus, they are suitable for a regular numerical evaluation. However, if both the source and field points are located on the interface, these expressions become singular. Then, a special treatment is necessary to evaluate these GFs. For brevity, we examine only the case where the source point is on the interface side of material 1. A detailed discussion for the 3D interfacial GF of elastostatics can be found in Ref. [17].

The singular interfacial GFs in the transformed domain are obtained by setting $Y_3 = y_3 = 0$ in Eqs. (30)–(35) and rearranging:

$$\tilde{\mathbf{u}}_1(k_1,k_2,y_3)\mathrm{e}^{-ik_\alpha Y_\alpha} = \tilde{\mathbf{u}}_2(k_1,k_2,y_3)\mathrm{e}^{-ik_\alpha Y_\alpha} = i\eta^{-1}(\mathbf{M}_1 - \bar{\mathbf{M}}_2)^{-1}\mathbf{f}, \tag{67}$$

$$\tilde{\mathbf{t}}_1(k_1,k_2,y_3)\mathrm{e}^{-ik_\alpha Y_\alpha} = \mathbf{M}_1(\mathbf{M}_1 - \bar{\mathbf{M}}_2)^{-1}\mathbf{f}, \tag{68}$$

$$\tilde{\mathbf{s}}_1(k_1,k_2,y_3)\mathrm{e}^{-ik_\alpha Y_\alpha} = \mathbf{N}_1(\mathbf{M}_1 - \bar{\mathbf{M}}_2)^{-1}\mathbf{f}, \tag{69}$$

$$\tilde{\mathbf{t}}_2(k_1,k_2,y_3)\mathrm{e}^{-ik_\alpha Y_\alpha} = \bar{\mathbf{M}}_2(\mathbf{M}_1 - \bar{\mathbf{M}}_2)^{-1}\mathbf{f}, \tag{70}$$

$$\tilde{\mathbf{s}}_2(k_1,k_2,y_3)\mathrm{e}^{-ik_\alpha Y_\alpha} = \bar{\mathbf{N}}_2(\mathbf{M}_1 - \bar{\mathbf{M}}_2)^{-1}\mathbf{f}. \tag{71}$$

It is noted that the transformed-domain displacement fields on the two sides of the interface are equal. Meanwhile, the transformed-domain traction, $\tilde{\mathbf{t}}$, exhibits a jump in the magnitude of **f** across the interface. This jump corresponds to the point force applied on the interface. The physical-domain counterpart, **t**, correspondingly exhibits a jump of $\mathbf{f}\delta(\mathbf{y}-\mathbf{Y})$ at the location of the point force. Furthermore, the transformed-domain in-plane stress, **s**, is in general different across the interface due to the materials mismatch.

The physical-domain interfacial GFs are derived as

$$u_{1i}(\mathbf{y}) = u_{2i}(\mathbf{y}) = \frac{1}{4\pi^2 r}\left\{\oint_{2\pi}\frac{[(\mathbf{M}_1 - \bar{\mathbf{M}}_2)^{-1}\mathbf{f}]_i}{\cos(\theta-\theta_0)}\mathrm{d}\theta + i\pi[(\mathbf{M}_1 - \bar{\mathbf{M}}_2)^{-1}\mathbf{f}]_i|_{\theta=\theta_0\pm\pi/2}\right\}, \tag{72}$$

$$t_{1i}(\mathbf{y}) = \frac{1}{4\pi^2 r^2}\left\{\oint_{2\pi}\frac{-[\mathbf{M}_1(\mathbf{M}_1 - \bar{\mathbf{M}}_2)^{-1}\mathbf{f}]_i}{\cos^2(\theta-\theta_0)}\mathrm{d}\theta \pm i\pi\frac{\partial[\mathbf{M}_1(\mathbf{M}_1 - \bar{\mathbf{M}}_2)^{-1}\mathbf{f}]_i}{\partial\theta}\bigg|_{\theta=\theta_0\pm\pi/2}\right\}, \tag{73}$$

$$s_{1i}(\mathbf{y}) = \frac{1}{4\pi^2 r^2}\left\{\oint_{2\pi}\frac{-[\mathbf{N}_1(\mathbf{M}_1 - \bar{\mathbf{M}}_2)^{-1}\mathbf{f}]_i}{\cos^2(\theta-\theta_0)}\mathrm{d}\theta \pm i\pi\frac{\partial[\mathbf{N}_1(\mathbf{M}_1 - \bar{\mathbf{M}}_2)^{-1}\mathbf{f}]_i}{\partial\theta}\bigg|_{\theta=\theta_0\pm\pi/2}\right\}, \tag{74}$$

$$t_{2i}(\mathbf{y}) = \frac{1}{4\pi^2 r^2}\left\{\oint_{2\pi}\frac{-[\bar{\mathbf{M}}_2(\mathbf{M}_1 - \bar{\mathbf{M}}_2)^{-1}\mathbf{f}]_i}{\cos^2(\theta-\theta_0)}\mathrm{d}\theta \pm i\pi\frac{\partial[\bar{\mathbf{M}}_2(\mathbf{M}_1 - \bar{\mathbf{M}}_2)^{-1}\mathbf{f}]_i}{\partial\theta}\bigg|_{\theta=\theta_0\pm\pi/2}\right\}, \tag{75}$$

$$s_{2i}(\mathbf{y}) = \frac{1}{4\pi^2 r^2}\left\{\oint_{2\pi}\frac{-[\bar{\mathbf{N}}_2(\mathbf{M}_1 - \bar{\mathbf{M}}_2)^{-1}\mathbf{f}]_i}{\cos^2(\theta-\theta_0)}\mathrm{d}\theta \pm i\pi\frac{\partial[\bar{\mathbf{N}}_2(\mathbf{M}_1 - \bar{\mathbf{M}}_2)^{-1}\mathbf{f}]_i}{\partial\theta}\bigg|_{\theta=\theta_0\pm\pi/2}\right\}. \tag{76}$$

The integrals are all taken in the sense of principle values. In the derivation of these expressions, the following formulas [2,21] are applied,

$$\int_0^\infty i\mathrm{e}^{-is\eta}\mathrm{d}\eta = \frac{1}{s} + i\pi\delta(s), \tag{77}$$

$$\int_0^\infty \eta\mathrm{e}^{-is\eta}\mathrm{d}\eta = -\frac{1}{s^2} + i\pi\frac{\partial\delta(s)}{\partial s}, \tag{78}$$

$$\delta(r\cos(\theta-\theta_0)) = \frac{\delta(\theta-\theta_0\pm\pi/2)}{r|\sin(\theta-\theta_0)|}. \tag{79}$$

4.2. Surface Green's function

Similarly, the surface GF where both $Y_3 = y_3 = 0$ is derived as follows:

$$\tilde{\mathbf{u}}(k_1,k_2,y_3)\mathrm{e}^{-ik_\alpha Y_\alpha} = i\eta^{-1}\mathbf{A}\mathbf{B}^{-1}\mathbf{f}, \tag{80}$$

$$\tilde{\mathbf{s}}(k_1,k_2,y_3)\mathrm{e}^{-ik_\alpha Y_\alpha} = \mathbf{C}\mathbf{B}^{-1}\mathbf{f}. \tag{81}$$

$$\mathbf{u}(\mathbf{y}) = \frac{1}{4\pi^2 r}\left\{\oint_{2\pi} \frac{\mathbf{A}\mathbf{B}^{-1}\mathbf{f}}{\cos(\theta-\theta_0)}\mathrm{d}\theta + i\pi[\mathbf{A}\mathbf{B}^{-1}\mathbf{f}]\Big|_{\theta=\theta_0\pm\pi/2}\right\}, \tag{82}$$

$$\mathbf{s}(\mathbf{y}) = \frac{1}{4\pi^2 r^2}\left\{\oint_{2\pi} \frac{-\mathbf{C}\mathbf{B}^{-1}\mathbf{f}}{\cos^2(\theta-\theta_0)}\mathrm{d}\theta \pm i\pi\frac{\partial[\mathbf{C}\mathbf{B}^{-1}\mathbf{f}]}{\partial\theta}\Big|_{\theta=\theta_0\pm\pi/2}\right\}, \tag{83}$$

for the lower-half-space case ($y_3 \le 0$), and

$$\tilde{\mathbf{u}}(k_1,k_2,y_3)\mathrm{e}^{-ik_\alpha Y_\alpha} = -i\eta^{-1}\bar{\mathbf{A}}\bar{\mathbf{B}}^{-1}\mathbf{f}, \tag{84}$$

$$\tilde{\mathbf{s}}(k_1,k_2,y_3)\mathrm{e}^{-ik_\alpha Y_\alpha} = -\bar{\mathbf{C}}\bar{\mathbf{B}}^{-1}\mathbf{f}. \tag{85}$$

$$\mathbf{u}(\mathbf{y}) = -\frac{1}{4\pi^2 r}\left\{\oint_{2\pi} \frac{\bar{\mathbf{A}}\bar{\mathbf{B}}^{-1}\mathbf{f}}{\cos(\theta-\theta_0)}\mathrm{d}\theta + i\pi[\bar{\mathbf{A}}\bar{\mathbf{B}}^{-1}\mathbf{f}]\Big|_{\theta=\theta_0\pm\pi/2}\right\}, \tag{86}$$

$$\mathbf{s}(\mathbf{y}) = \frac{1}{4\pi^2 r^2}\left\{\oint_{2\pi} \frac{\bar{\mathbf{C}}\bar{\mathbf{B}}^{-1}\mathbf{f}}{\cos^2(\theta-\theta_0)}\mathrm{d}\theta \pm i\pi\frac{\partial[-\bar{\mathbf{C}}\bar{\mathbf{B}}^{-1}\mathbf{f}]}{\partial\theta}\Big|_{\theta=\theta_0\pm\pi/2}\right\}, \tag{87}$$

for the upper-half-space case ($y_3 \ge 0$). The traction, $\mathbf{t}$, is equal to zero except at the location of the point force, as imposed as the boundary condition to the half-spaces.

5. Numerical examples

In this section, we apply the previous formulation to examine the 3D steady-state fields in AlN/InN bimaterials subjected to a steadily moving point force. Both materials are transversely isotropic. By AlN/InN bimaterials, we mean that the lower half-space is occupied by AlN, and the upper half-space by InN. We further mention that both materials have a strong piezoelectric coupling [22]. In this paper, however, only their elastic response is considered. The material constants in the reduced notation (i.e. $C_{i'j'} - C_{ijkl}$ with $i' - ij$ and $j' - kl$: 1–11; 2–22; 3–33; 4–23; 5–31; 6–12) are given by $C_{11} = 410$ GPa, $C_{12} = 149$ GPa, $C_{13} = 99$ GPa, $C_{33} = 389$ GPa, $C_{44} = 125$ GPa for AlN [23], and $C_{11} = 190$ GPa, $C_{12} = 104$ GPa, $C_{13} = 121$ GPa, $C_{33} = 182$ GPa, $C_{44} = 10$ GPa for InN [24]. The mass density is 3.23 kg/m^3 for AlN, and 6.81 kg/m^3 for InN, from the same references as above. The isotropy-symmetry axis of the materials is taken to be along the y_3-axis. Therefore, an in-plane rotation of the horizontally moving point force vector would not change the characteristics in the response field.

Let us assume that a point force is applied at a depth of 10 mm below the interface and moves steadily along the x_1-direction in the AlN half-space. The magnitude of the point force is 1 N, and the force can be along either axis. The origin of the moving Cartesian reference frame is placed right above the moving point force. The steady-state fields along the interface over the point force are calculated for three different magnitudes of the point-force velocity, i.e. $|\boldsymbol{v}| = 0$, 500, and 1000 m/s. At a speed of slightly more than 1210 m/s, two of the six eigenvalues of Eq. (10) become real and the first transonic wave propagation is reached [1].

Figs. 2–10 show the contours of the stress component σ_{33} and hydrostatic stress $\sigma_{kk}(=\sigma_{11}+\sigma_{22}+\sigma_{33})$ due to the point force applied along the x_1-, x_2-, and x_3- axes, respectively. The unit of the stress quantities is Pa. We remark that the stress component σ_{33} does not change across the interface because of the continuity condition of traction imposed in the bimaterial GF; however, due to the materials mismatch, the hydrostatic stress σ_{kk} jumps across the interface. The hydrostatic stress on the AlN side of the interface is indicated by σ_{kk}^- and that on the InN side by σ_{kk}^+.

From these figures, we have observed the following features:

1. For the static case of $|\mathbf{v}| = 0$, a comparison of Figs. 2 and 5 shows that a switch of the direction of the point force between the in-plane axes causes no change in the response fields after a corresponding in-plane rotation of 90°. Furthermore, in Fig. 8, when the point force is applied along the x_3-axis, the contours of the responses are circular. These features indicate that the elastostatic fields are invariant with an in-plane rotation of the point-force direction. This invariance is due to the fact that the isotropy-symmetry axis of the materials is along the y_3-axis. However, when $|\mathbf{v}| > 0$, this rotational symmetry breaks down—the point-force-induced fields are altered by the inertial effect.
2. The break-down of the rotational symmetry in the steady-state responses is observed by comparing Figs. 3 and 6 for velocity at $|\mathbf{v}| = 500$ m/s, and Figs. 4 and 7 at $|\mathbf{v}| = 1000$ m/s. When the point-force is along the x_3-axis, the circular contours are distorted for the velocity at $|\mathbf{v}| = 500$ m/s (Fig. 9) and further at $|\mathbf{v}| = 1000$ m/s (Fig. 10).
3. The materials mismatch between AlN and InN causes large difference in the hydrostatic stress, σ_{kk}^- and σ_{kk}^+. When the point force is applied along the in-plane axes, the hydrostatic stress has two pairs of hill–valley variation in AlN but only one pair of hill–valley variation in InN (see, e.g. Figs. 2–4). The magnitudes are very different, respectively at about 500 and 150 Pa (Figs. 2–4). When the point force is directed along the x_3-axis, the hydrostatic stresses differ by over one order of magnitude, and have opposite signs (Fig. 8). The stress does not change much with increasing point-force speed in AlN, but changes significantly in InN. The peak value of σ_{kk}^+ in InN, which is at the origin (0,0,0), is equal to 63.2 Pa at $|\mathbf{v}| = 0$, 63.3 Pa at $|\mathbf{v}| = 500$ m/s, and 276 Pa at $|\mathbf{v}| = 1000$ m/s (Figs. 8c, 9c, 10c). Furthermore,

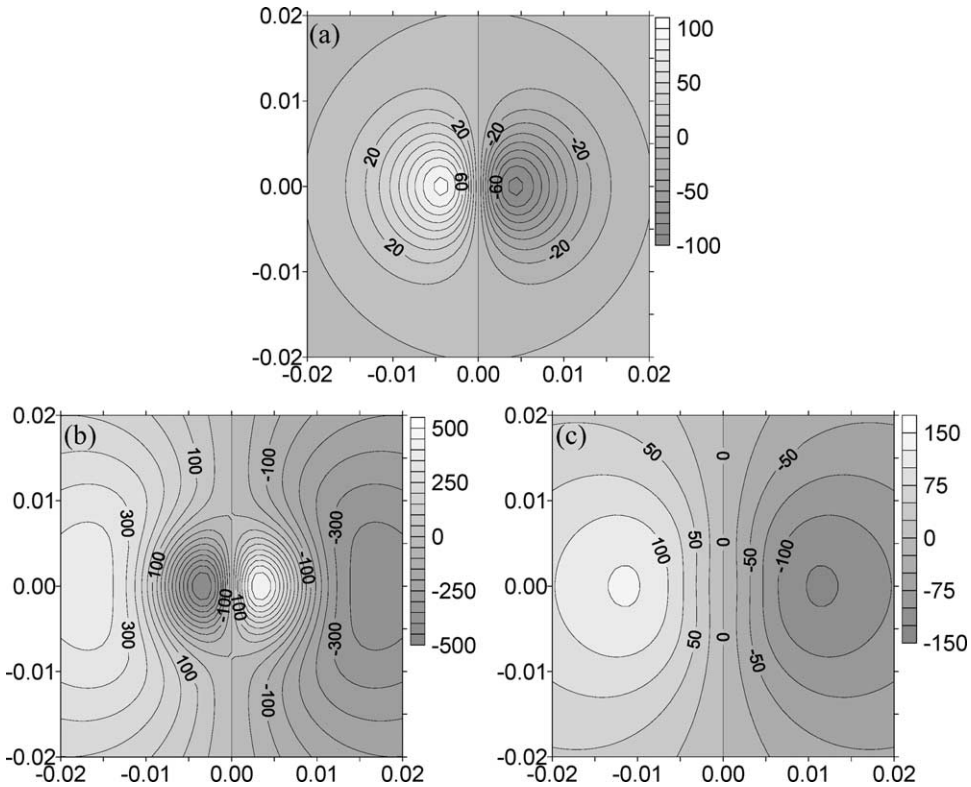

Fig. 2. Stress distributions on the interface due to a point force along the x_1-direction with velocity $|\mathbf{v}| = 0$: (a) σ_{33}; (b) σ_{kk}^{-}; (c) σ_{kk}^{+} (Pa).

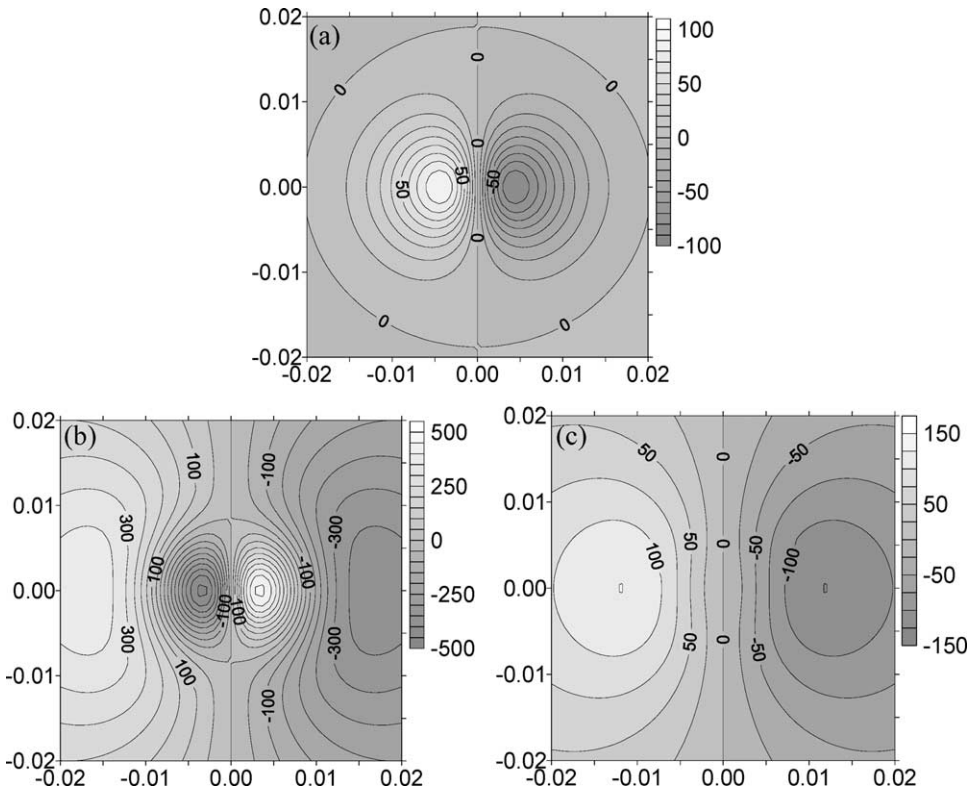

Fig. 3. Stress distributions on the interface due to a point force along the x_1-direction with velocity $|\mathbf{v}| = 500$S m/s: (a) σ_{33}; (b) σ_{kk}^{-}; (c) σ_{kk}^{+} (Pa).

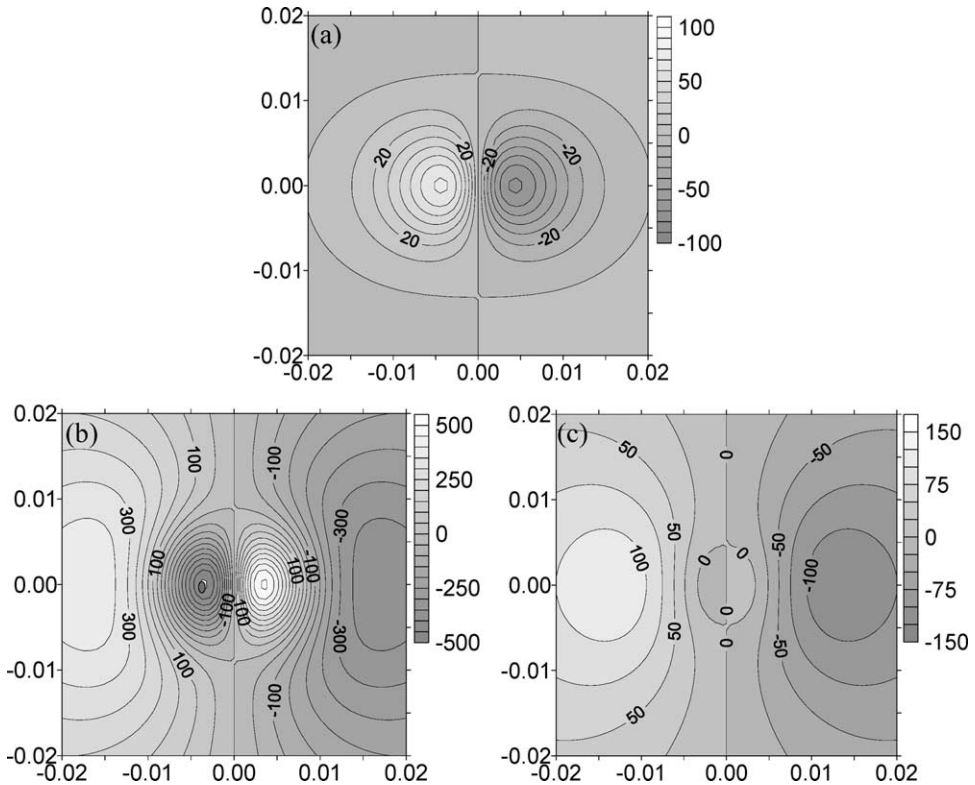

Fig. 4. Stress distributions on the interface due to a point force along the x_1-direction with velocity $|\mathbf{v}| = 1000$ m/s: (a) σ_{33}; (b) σ_{kk}^{-}; (c) σ_{kk}^{+} (Pa).

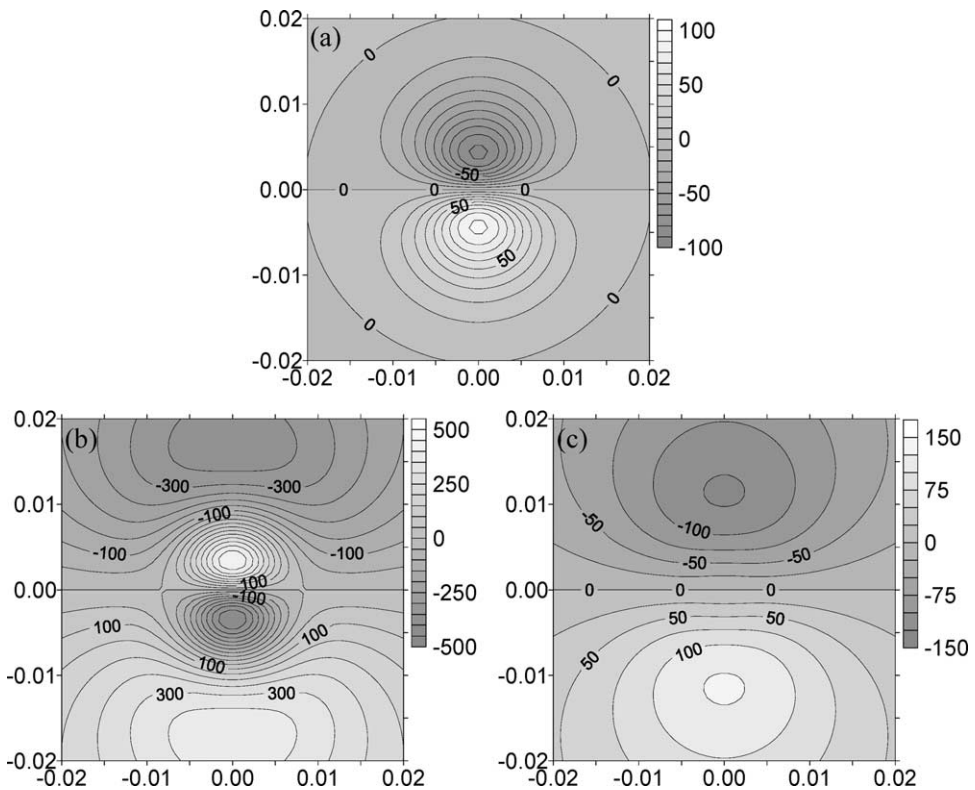

Fig. 5. Stress distributions on the interface due to a point force along the x_2-direction with velocity $|\mathbf{v}| = 0$: (a) σ_{33}; (b) σ_{kk}^{-}; (c) σ_{kk}^{+} (Pa).

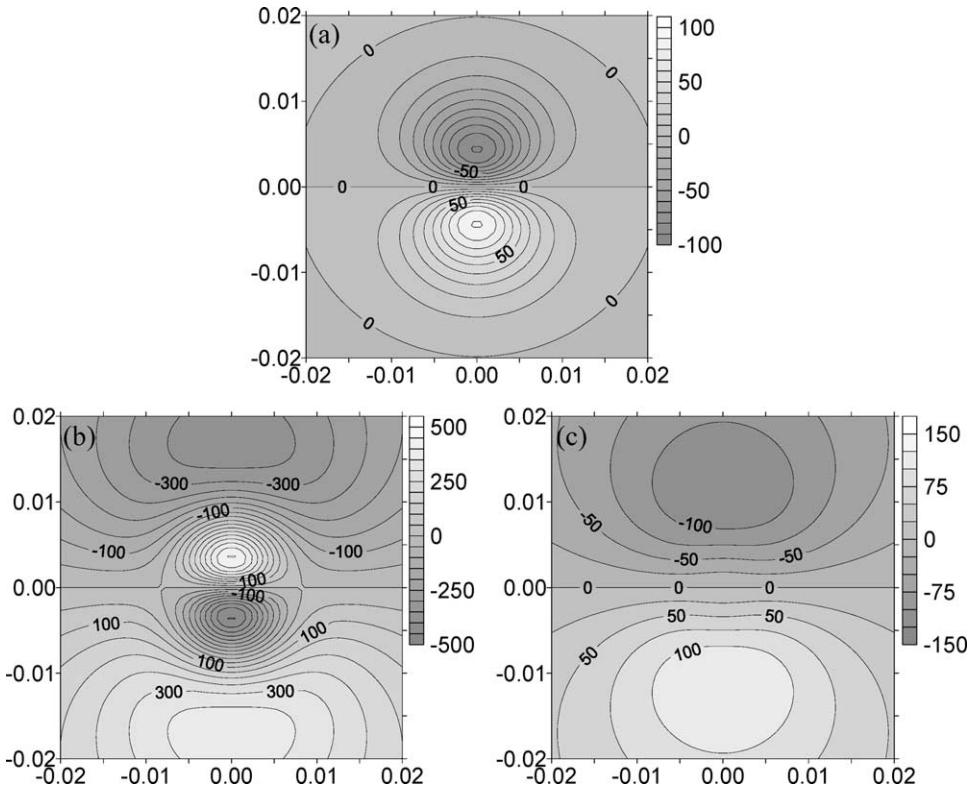

Fig. 6. Stress distributions on the interface due to a point force along the x_2-direction with velocity $|\mathbf{v}| = 500$ m/s: (a) σ_{33}; (b) σ_{kk}^{-}; (c) σ_{kk}^{+} (Pa).

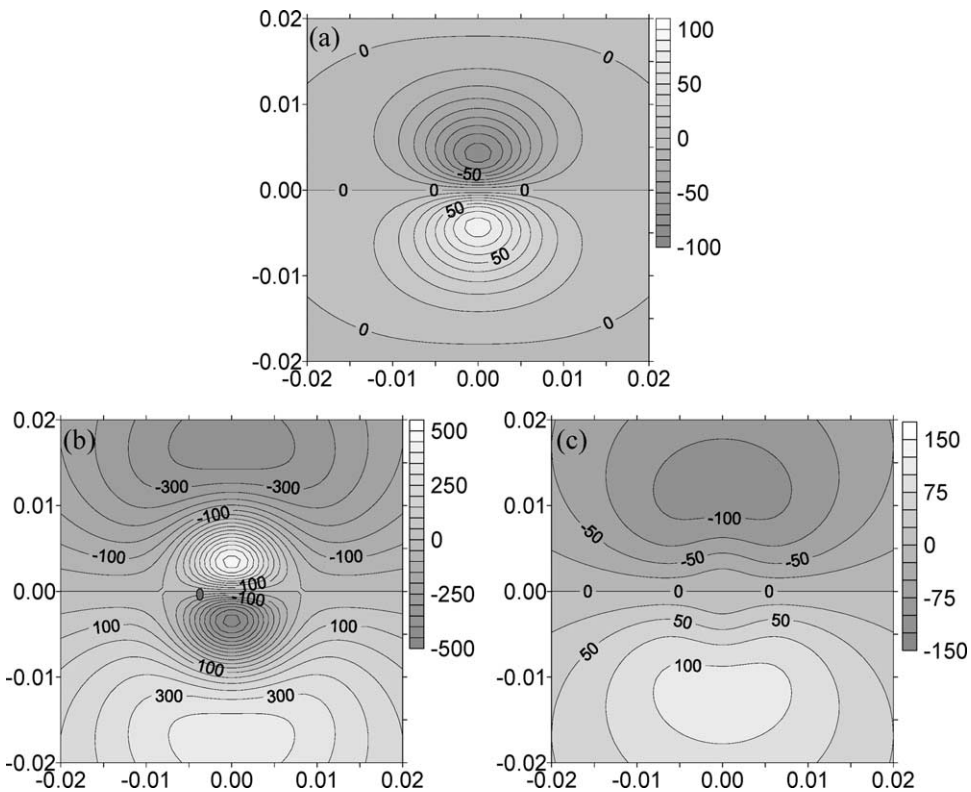

Fig. 7. Stress distributions on the interface due to a point force along the x_2-direction with velocity $|\mathbf{v}| = 1000$ m/s: (a) σ_{33}; (b) σ_{kk}^{-}; (c) σ_{kk}^{+} (Pa).

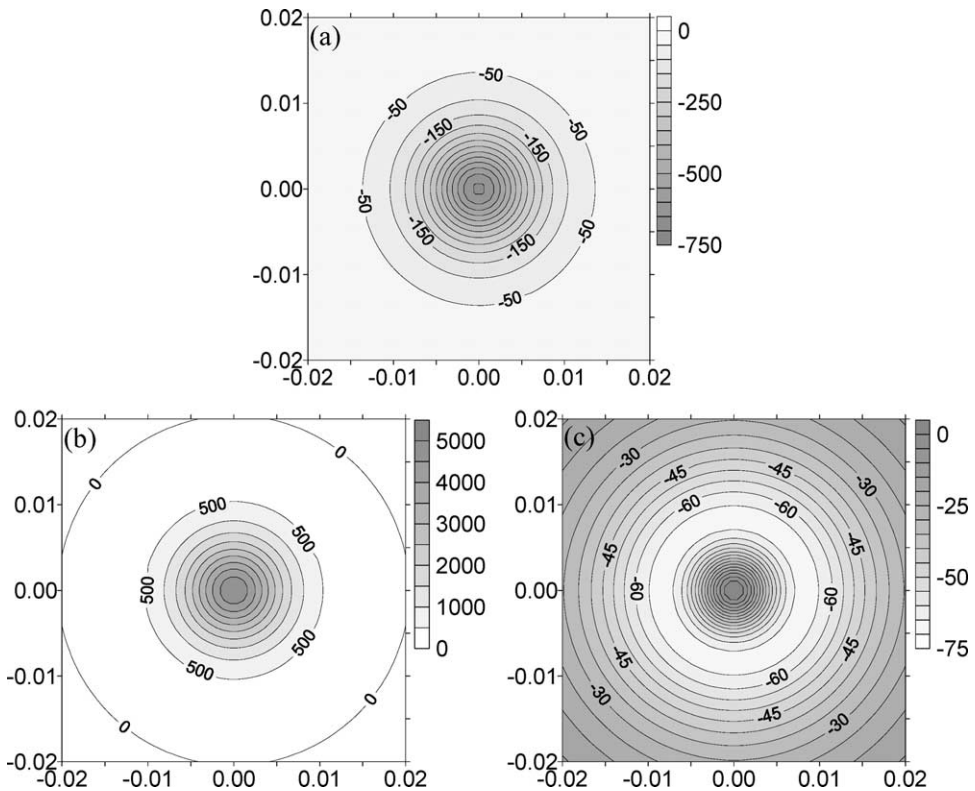

Fig. 8. Stress distributions on the interface due to a point force along the x_3-direction with velocity $|\mathbf{v}| = 0$: (a) σ_{33}; (b) σ_{kk}^{-}; (c) σ_{kk}^{+} (Pa).

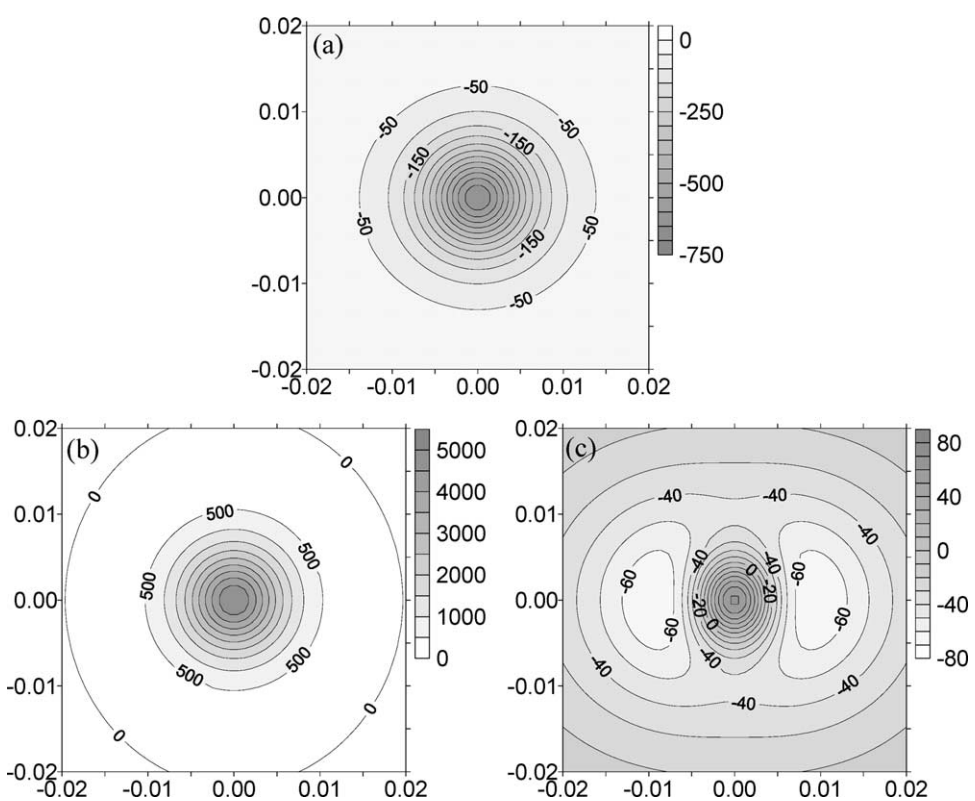

Fig. 9. Stress distributions on the interface due to a point force along the x_3-direction with velocity $|\mathbf{v}| = 500$ m/s: (a) σ_{33}; (b) σ_{kk}^{-}; (c) σ_{kk}^{+} (Pa).

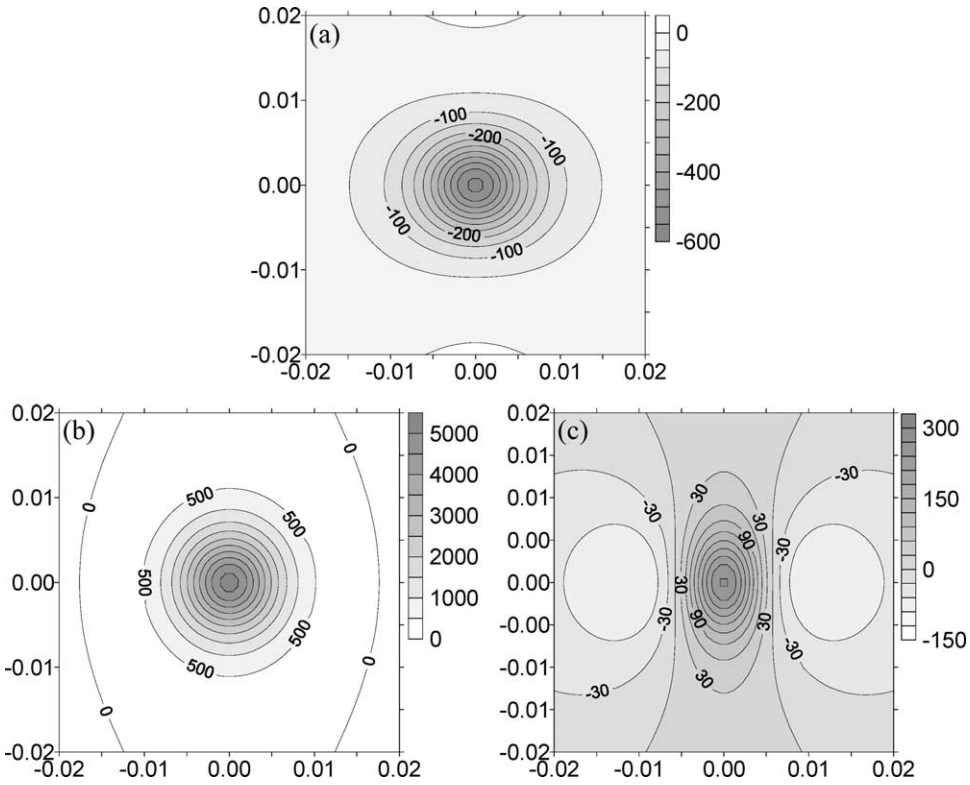

Fig. 10. Stress distributions on the interface due to a point force along the x_3-direction with velocity $|\mathbf{v}| = 1000$ m/s: (a) σ_{33}; (b) σ^{-}_{kk}; (c) σ^{+}_{kk} (Pa).

at nonzero $|\mathbf{v}|$, two satellite minima are formed for σ^{+}_{kk} beside the central peak in the contour plots.

6. Conclusions

We have presented the 3D GFs of a steadily moving point source in linear anisotropic elastic half-spaces and bimaterials. The GFs are obtained within the framework of generalized Stroh formalism and the 2D Fourier transforms for the subsonic case.

Numerical examples of the AlN/InN bimaterial subjected to a steadily moving point force are carried out to demonstrate the significant effects of wave velocity on the stress fields. We observed that, in general, when the wave velocity $|\mathbf{v}| > 0$, the features in the contour plots of, for example, the stress component σ_{33} and hydrostatic stress σ_{kk}, can be distorted significantly. Furthermore, the magnitude of the stress field increases with increasing wave velocity $|\mathbf{v}|$. For example, the peak value of the hydrostatic stress in InN may increase by a factor between 4 and 5 when the wave velocity $|\mathbf{v}|$ increases from 500 to 1000 m/s.

While the supersonic case will be investigated in the future, the numerical results for the subsonic case clearly show the remarkable difference in the stress fields due to the static and steady-state point sources. In the other words, the stress field in the static case should, in general, not be applied to the steady-state case. This could particularly be useful for the stress analysis in structures under steady-state loading, such as highways under cars and railways under trains. Furthermore, the present GF solutions can be incorporated into a steady-state boundary integral equation to analyze more complicated practical problems.

Acknowledgements

BY was financially sponsored by Kent State University and Massachusetts Institute of Technology through the NSF project #0121545, and EP by University of Akron.

Appendix A

In this Appendix A, we derive the explicit steady-state Green's displacements in an anisotropic elastic full-space. The same frames are established as in the text. The Green's displacements, G_{kp}, are the fundamental solutions of Eq. (4) caused by a unit point force. This Green's tensor is defined by the partial differential equations

$$C^{*}_{ijkl} G_{kp,li}(\mathbf{y}) = -\delta_{jp}\delta(\mathbf{y}), \tag{A1}$$

where δ_{jp} is the Kronecker delta, the first index, k, of the Green's tensor denotes the displacement component, and the second, p, denotes the direction of the point force.

To derive the Green's tensor, we resort to the following plane representation of the Dirac delta function [18,19]:

$$\delta(\mathbf{y}) = -\frac{1}{8\pi^2}\Delta\int_{\Omega}\frac{\delta(\mathbf{n}\cdot\mathbf{y})}{|\mathbf{n}|^2}\mathrm{d}\Omega(\mathbf{n}), \tag{A2}$$

where $\mathbf{n}$ is a vector variable with components (n_1, n_2, n_3), and $\Omega(\mathbf{n})$ is a closed surface enclosing the origin. The integral is taken over all planes defined by $\mathbf{n}\times\mathbf{y} = 0$. The dot '·' denotes the inner product, and Δ is the 3D Laplacian operator.

We now introduce a 3×3 matrix

$$\Gamma_{jk}(\mathbf{n}) = C^*_{ijkq}n_i n_q, \tag{A3}$$

and denote its inverse by $\Gamma^{-1}_{jk}(\boldsymbol{n})$. Integrating $\Gamma^{-1}_{jk}(\boldsymbol{n})\delta(\boldsymbol{n}\cdot\mathbf{y})$ with respect to $\boldsymbol{n}$, taking its second derivatives with respect to y_i, and multiplying the result by the extended stiffness matrix C^*_{ijkl}, we then arrive at the following important identity:

$$C^*_{ijkq}\frac{\partial^2}{\partial y_i\partial y_q}\int_{\Omega}\Gamma^{-1}_{jk}(\mathbf{n})\delta(\mathbf{n}\cdot\mathbf{y})\mathrm{d}\Omega(\mathbf{n}) = \delta_{jp}\Delta\int_{\Omega}\frac{\delta(\mathbf{n}\cdot\mathbf{y})}{|\mathbf{n}|^2}\mathrm{d}\Omega(\mathbf{n}). \tag{A4}$$

Making use of the plane representation (A2), this equation can be rewritten as

$$C^*_{ijkq}\frac{\partial^2}{\partial y_i\partial y_q}\int_{\Omega}\Gamma^{-1}_{jk}(\mathbf{n})\delta(\mathbf{n}\cdot\mathbf{y})\mathrm{d}\Omega(\mathbf{n}) = -8\pi^2\delta_{jp}\delta(\mathbf{y}). \tag{A5}$$

Comparing Eq. (A5) to (A1), we finally obtain the following integral expression for the Green's displacement tensor

$$G_{jk}(\mathbf{y}) = \frac{1}{8\pi^2}\int_{\Omega}\Gamma^{-1}_{jk}(\mathbf{n})\delta(\mathbf{n}\cdot\mathbf{y})\mathrm{d}\Omega(\mathbf{n}), \tag{A6}$$

or,

$$G_{jk}(\mathbf{y}) = \frac{1}{8\pi^2}\int_{\Omega}\frac{A_{jk}(\mathbf{n})}{D(\mathbf{n})}\delta(\mathbf{n}\cdot\mathbf{y})\mathrm{d}\Omega(\mathbf{n}), \tag{A7}$$

where $A_{jk}(\mathbf{n})$ and $D(\mathbf{n})$ are, respectively, the adjoint matrix and determinant of $\Gamma_{jk}(\mathbf{n})$.

The integral expression (A7) for the Green's tensor can actually be transformed to a 1D infinite integral and the result can then be reduced to a summation of three residues. This is achieved by expressing the vector variable $\mathbf{n}$ in terms of a new, orthogonal, and normalized system $(O;\mathbf{e},\mathbf{p},\mathbf{q})$, instead of the space-fixed Cartesian coordinates $(O;y_1,y_2,y_3)$. The new base $(\mathbf{e},\mathbf{p},\mathbf{q})$ are chosen as the following

$$\mathbf{e} = \mathbf{y}/r;\quad r = |\mathbf{y}|. \tag{A8}$$

Now let $\mathbf{v}$ be an arbitrary unit vector different from $\mathbf{e}(\mathbf{v}\neq\mathbf{e})$; the two unit vectors orthogonal to $\mathbf{e}$ can then be selected as

$$\mathbf{p} = \frac{\mathbf{e}\times\mathbf{v}}{|\mathbf{e}\times\mathbf{v}|};\quad \mathbf{q} = \mathbf{e}\times\mathbf{p}. \tag{A9}$$

It should be emphasized that $\mathbf{e}\times\mathbf{v}$ should be normalized so that $\mathbf{p}$ is a unit vector.

In the new reference system $(O;\mathbf{e},\mathbf{p},\mathbf{q})$, we let the vector variable $\mathbf{n}$ be expressed as

$$\mathbf{n} = \xi\mathbf{p} + \zeta\mathbf{q} + \eta\mathrm{e}. \tag{A10}$$

It is clear then that

$$\mathbf{n}\cdot\mathbf{x} = \mathbf{p}\cdot\mathbf{y}\xi + \mathbf{q}\cdot\mathbf{y}\zeta + \mathbf{e}\cdot\mathbf{y}\eta = r\eta. \tag{A11}$$

Therefore, in terms of the reference system $(O;\mathbf{e},\mathbf{p},\mathbf{q})$, Eq. (A7) becomes

$$G_{jk}(\mathbf{y}) = \frac{1}{8\pi^2}\int_{\Omega}\frac{A_{jk}(\xi\mathbf{p}+\zeta\mathbf{q}+\eta\mathbf{e})}{D(\xi\mathbf{p}+\zeta\mathbf{q}+\eta\mathbf{e})}\delta(r\eta)\mathrm{d}\Omega(\xi,\zeta,\eta), \tag{A12}$$

where Ω is again a closed surface enclosing the origin $(\xi,\zeta,\eta) = (0,0,0)$. Carrying out the integration with respect to η yields

$$G_{jk}(\mathbf{y}) = \frac{1}{4\pi^2 r}\int_{-\infty}^{\infty}\frac{A_{jk}(\mathbf{p}+\zeta\mathbf{q})}{D(\mathbf{p}+\zeta\mathbf{q})}\mathrm{d}\zeta. \tag{A13}$$

We now look at the matrix $\Gamma_{jk}(\mathbf{p}+\zeta\mathbf{q})$ and its determinant $D(\mathbf{p}+\zeta\mathbf{q})$. It turns out that the matrix Γ_{jk} can actually be expressed by the Stroh formalism. That is,

$$\Gamma(\mathbf{p}+\zeta\mathbf{q}) \equiv \mathbf{Q} + \zeta(\mathbf{R}+\mathbf{R}^{\mathrm{T}}) + \zeta^2\mathbf{T}, \tag{A14}$$

where

$$Q_{ik} = C^*_{jiks}p_j q_s,\ R_{ik} = C^*_{jiks}p_j q_s,\ T_{ik} = C^*_{jiks}q_j q_s. \tag{A15}$$

The determinant $D(\mathbf{p}+\zeta\mathbf{q})$ is a sixth-order polynomial equation of ζ and has six roots. For the velocity constraint assumed in this paper, three of them are the conjugate of the remainder. These roots can be found either by expanding the determinant $D(\mathbf{p}+\zeta\mathbf{q})$ into the polynomial, or by finding the six eigenvalues of the following linear eigen equation [1]:

$$\begin{bmatrix}\mathbf{N}_1 & \mathbf{N}_2\\ \mathbf{N}_3 & \mathbf{N}_1^{\mathrm{T}}\end{bmatrix}\begin{bmatrix}\mathbf{a}\\ \mathbf{b}\end{bmatrix} = \zeta\begin{bmatrix}\mathbf{a}\\ \mathbf{b}\end{bmatrix}, \tag{A16}$$

where

$$\mathbf{N}_1 = -\mathbf{T}^{-1}\mathbf{R}^{\mathrm{T}},\ \mathbf{N}_2 = \mathbf{T}^{-1},\ \mathbf{N}_3 = \mathbf{R}\mathbf{T}^{-1}\mathbf{R}^{\mathrm{T}} - \mathbf{Q}, \tag{A17}$$

and the eigenvectors $\mathbf{a}$ and $\mathbf{b}$ are the coefficients of the extended displacement and traction vectors.

Assume that $\mathrm{Im}\zeta_m > 0, m = 1,\ 2,\ 3$ and $\zeta_m{}^*$ is the conjugate of ζ_m, the extended Green's displacement can

finally be expressed explicitly as

$$G_{jk}(\mathbf{y}) = -\frac{\mathrm{Im}}{2\pi r}\sum_{m=1}^{3}\frac{A_{jk}(\mathbf{p}+\zeta_m\mathbf{q})}{a_{11}(\zeta_m-\zeta_m^*)\prod_{\substack{k=1\\k\neq m}}^{3}(\zeta_m-\zeta_k)(\zeta_m-\zeta_k^*)} \tag{A18}$$

where $a_{11} = \det(\mathbf{T})$ is the coefficient of ζ^6.

This is the explicit expression for the steady-state Green's displacement tensor in an anisotropic and elastic infinite space. The Green's strains and stresses can be found from the Green's displacements numerically as in Refs. [18,19].

References

[1] Ting TCT. Anisotropic elasticity. Oxford: Oxford University Press; 1996.

[2] Pan E, Yuan FG. Three-dimensional Green's functions in anisotropic bimaterials. Int J Solids Struct 2000;37:5329–51.

[3] Pan E. Mindlin's problem for an anisotropic piezoelectric half space with general boundary conditions. Proc R Soc Lond A 2002;458: 181–208.

[4] Yang B, Pan E. Three-dimensional Green's functions in anisotropic trimaterials. Int J Solids Struct 2002;39:2235–55.

[5] Yang B, Pan E. Efficient evaluation of three-dimensional Green's functions in anisotropic elastostatic multilayered composites. Eng Anal Bound Elements 2002;26:355–66.

[6] Wang W, Ishikawa H. A method for linear elasto-static analysis of multi-layered axisymmetrical bodies using Hankel's transform. Comp Mech 2001;27:474–83.

[7] Berger JR, Tewary VK. Greens functions for boundary element analysis of anisotropic bimaterials. Eng Anal Bound Elements 2001; 25:279–88.

[8] Pavlou DG. Green's function for the biomaterial elastic solid containing interface annular crack. Eng Anal Bound Elements 2002; 26:845–53.

[9] Tewary VK, Fortunko CM. A computationally efficient representation for propagation of elastic waves in anisotropic solids. J Acoust Soc Am 1992;91:1888–96.

[10] Wang CY, Achenbach JD. Three-dimensional time-harmonic elastodynamic Green's functions for anisotropic solids. Proc R Soc Lond A 1995;449:441–58.

[11] Wu KC. Extension of Stroh's formalism to self-similar problems in two-dimensional elastodynamics. Proc R Soc Lond A 2000;456: 869–90.

[12] Achenbach JD. Wave propagation in elastic solids. New York: North-Holland Publishing Company; 1973.

[13] Graff KF. Wave motion in elastic solids. Ohio: Ohio State University Press; 1975.

[14] Verruijt A, Cordova CC. Moving loads on an elastic half-plane with hysteretic damping. ASME J Appl Mech 2001;68:915–22.

[15] Lykotrafitis G, Georgiadis HG. The three-dimensional steady-state thermo-elastodynamic problem of moving sources over a half space. Int J Solids Struct 2003;40:899–940.

[16] Andersen L, Nielsen SRK. Boundary element analysis of the steady-state response of an elastic half-space to a moving force on its surface. Eng Anal Bound Elements 2003;27:23–38.

[17] Pan E, Yang B. Three-dimensional interfacial Green's functions in anisotropic bimaterials. Appl Mathl Modelling 2003;27:307–26.

[18] Pan E, Tonon F. Three-dimensional Green's functions in anisotropic piezoelectric solids. Int J Solids Struct 2000;37:943–58.

[19] Tonon F, Pan E, Amadei B. Green's functions and boundary element method formulation for 3D anisotropic media. Computers Struct 2001;79:469–82.

[20] Pan E. Three-dimensional Green's functions in an anisotropic half space with general boundary conditions. ASME J Appl Mech 2003; 70:180–90.

[21] Barnett DM, Lothe J. Line force loadings on anisotropic half-spaces and wedges. Phys Norvegica 1975;8:13–22.

[22] Pan E, Yang B. Elastic and piezoelectric fields in a substrate AlN due to a buried quantum dot. J Appl Phys 2003;93:2435–9.

[23] Goldberg Yu. Aluminum nitride. In: Levinshtein ME, Rumyantsev SL, Shur MS, editors. Properties of advanced semiconductor materials. New York: Wiley; 2001.

[24] Zubrilov A. Indium nitride. In: Levinshtein ME, Rumyantsev SL, Shur MS, editors. Properties of advanced semiconductor materials. New York: Wiley; 2001.